Applied Soft Computing 48 (2016) 124–136

Contents lists available at ScienceDirect

Applied Soft Computing

journal homepage: www.elsevier.com/locate/asoc

Robust parameter design for the micro-BGA stencil printing process using a fuzzy logic-based Taguchi method

Tsung-Nan Tsai [a,*], Mika Liukkonen [b]

[a] Department of Distribution Management, Shu-Te University, 59, Hengshan Rd. Yenchao, Kaohsiung, Taiwan
[b] University of Eastern Finland, Department of Environmental Science, P.O. Box 1627, FIN-70211 Kuopio, Finland

ARTICLE INFO

Article history:
Received 12 January 2016
Received in revised form 29 May 2016
Accepted 16 June 2016
Available online 30 June 2016

Keywords:
Fuzzy logic
Surface mount technology
Stencil printing
Ball grid array
Printed circuit board
Neural network
Genetic algorithm

ABSTRACT

Solder paste is the main soldering material used to form strong solder joints between printed circuit boards (PCB) and surface mount devices in the surface mount assembly (SMA). On average 60% of end-of-line soldering defects can be attributed to inadequate performance of solder paste stencil printing. Recently, lead-free solder paste has been adopted by electronics manufacturers in compliance with the RoHS directive. However, soldering defects in the ball grid array (BGA) packages used in lead-free SMA have become more prevalent and are difficult to detect. In this study, a fuzzy logic-based Taguchi method is proposed to optimize the fine-pitch stencil printing process with multiple quality characteristics for the micro ball grid array (micro-BGA) packages using a lead-free solder paste. A structured data set is first collected from an L_{18} ($2^1 \times 3^7$) fractional factorial design experiment, followed by multi-response optimizations and analysis of variance (ANOVA) for identifying significant factors. The optimization performance gained by the proposed fuzzy logic-based Taguchi method is compared with the results of other two hybrid methods including a combination of neural networks and genetic algorithms, and the integration of the response surface methodology with a desirability function. The confirmation experiments show that the proposed fuzzy logic-based Taguchi method outperforms the other two methods in terms of the signal-to-noise ratios and process capability index.

1. Introduction

Surface mount technology (SMT) is the primary method used for the fabrication of many modern electronic products. The surface mount assembly (SMA) process consists of three sub-processes, including solder paste stencil printing application, component placement, and solder reflow, to form strong metal solder joints between the printed circuit board (PCB) and surface mount devices (SMDs). Changing consumer preferences have driven product designers to continue the move towards miniaturization that makes SMA process more complicated to control. Especially, the solder paste stencil printing is recognized as the most difficult process for quality assurance in electronic assembly, and averagely 60% of end-of-line soldering defects can be attributed to poor stencil printing performance [34,46].

The purpose of the stencil printing process is to consistently deposit the desired amount of solder paste in the appropriate form at the correct position for every printing cycle [6]. Taking the BGA package as an example of stencil printing, in the first step, air pressure is applied to force the solder paste to roll to the front of the squeegee blade and fill in the stencil apertures, as displayed in Fig. 1(a). The squeegee travels across the surface of the stencil to transfer and deposit solder paste onto the corresponding PCB pads for the BGA package after the stencil is released, as depicted in Fig. 1(b). After that, the BGA package is placed on the corresponding printed pads using a placement machine in the component placement stage, as shown in Fig. 1(c). Finally, the solder paste is heated and solder joints are formed through a reflow oven.

The stencil printing performance is influenced by many variables, including stencil aperture design, solder paste properties, tool selection, and printing method [40]. The stencil printing factors are frequently considered by researchers and process practitioners, as summarized in Table 1. For examples, Coleman [10] and Smith [43] revealed that the amount of solder paste deposited is directly restricted by the stencil aperture area ratio and stencil thickness. The squeegee pressure and speed, as well as the speed used to separate the stencil from the PCB also have consolidated effects on the uniform formation of paste bricks [34,45]. Too low a squeegee pressure can leave a thin film of solder paste on the stencil surface,

* Corresponding author.
E-mail addresses: tntsai@stu.edu.tw (T.-N. Tsai), mika.liukkonen@uef.fi (M. Liukkonen).

http://dx.doi.org/10.1016/j.asoc.2016.06.020
1568-4946/

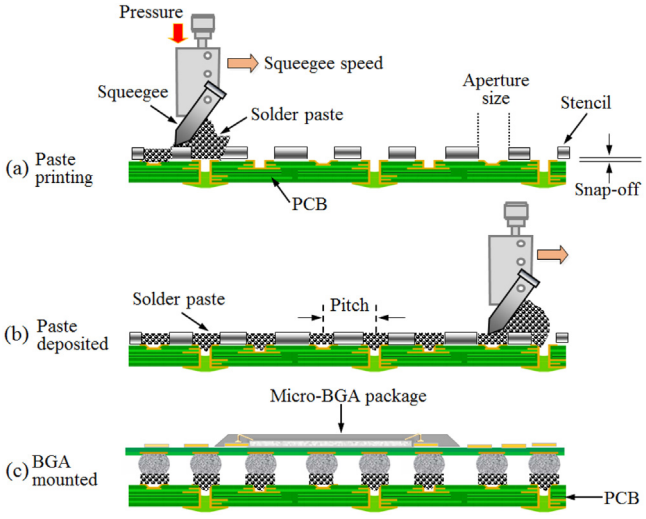

Fig. 1. Stencil printing and placement of a BGA package.

Table 1
Summary of the mostly considered stencil printing factors.

Stencil printing factors	Publications
Stencil and aperture designs	[1,10,43,45,46,34,40]
Solder paste properties	[1,5,7,6,18,20,22,43,45,54]
Squeegee pressure	[5,6,26,34,40,44,46]
Squeegee speed	[5,6,26,34,40,45,46]
Separation speed	[5,6,10,34,40]
Stencil wiping and cleaning frequency	[1,5,6,15]
Snap-off height	[22,43,34,45,46]

conversely too high a squeegee pressure may yield scooped paste prints and deposit irregular amounts of solder paste [44]. Furthermore, too high a separation speed may pull the solder paste out of the aperture and generate an uneven paste brick surface [10]. More frequent wiping and cleaning the bottom of the stencil may produce better print quality and registration [15], however it increases printing cycle time.

Solder paste is the main soldering material used in the SMA. It is not possible to continue using certain hazardous materials in electrical and electronic equipment due to the restrictions of the hazardous substances (RoHS) directive. As a result, most electronics manufacturers have gradually replaced the traditional tin-lead solder paste (i.e., Sn63/Pb37) by a lead-free alternative. The Sn-Ag-Cu (SAC solder alloy, e.g., Sn96.5/Ag3.0/Cu0.5) family of lead-free solder alloys are the most promising candidate for the replacement of eutectic Tin-lead ones to adapt in miniaturization technologies and are most commonly utilized in modern electronics industry [22]. However, the performance of the lead-free solder paste differs from its counterparts because of differences in the materials properties. A major influence under investigations for melting temperature of lead-free alloys are 30–40 °C higher than Tin-lead solder in the solder reflow process. The main differences between leaded (Sn63Pb37) and lead-free (Sn96.5/Ag3.0/Cu0.5) solder alloys concerned by process practitioners are summarized in Table 2 [18,54]. Recent studies have indicated that the properties of the lead-free solder paste and the fine-pitch SMDs are the two most important factors to consider in improving soldering quality [6]. Therefore, a good understanding of the soldering paste properties is crucial to process practitioners who can conduct the necessary stencil printing process changes and reduce soldering defects, and increase lead-free assembly reliability.

The soldering defects became even more prevalent after the BGA packages were assembled using lead-free alloys and have often been difficult to detect [39]. An inappropriate amount of solder paste for a specific micro-BGA package can lead to several soldering defects, such as bridging, insufficient wetting, and cold solder joints. Furthermore, an imbalance of solder paste deposits on the BGA packages can generate end-of-line soldering defects, such as opening, balling, and head-in-pillow defects [40]. The wetting performance of the lead-free SMA may not be as good as that of the tin-lead one, being particularly sensitive to paste-to-pad misalignments or centroid offsets, which can lead to serious soldering defects for micro-BGA packages [20,43].

In practice, engineers usually utilize a time-consuming trial-and-error search for printing parameters to find acceptable printing quality, and this can dramatically increase manufacturing costs. Although the soldering defects for micro-BGA packages can be repaired manually, however, it is costly to increase inspection and quality recovery efforts. Thus, optimization of the fine-pitch micro-BGA stencil printing process with multiple quality characteristics is necessary for lead-free SMA to become a more efficient and cost-effective strategy, especially, for improving the stencil printing process performance to achieve robust solder joints without jeopardizing the downstream processing steps [40].

The remainder of this paper is organized as follows. The literature is reviewed and the methodologies used to optimize a stencil printing process with multiple quality characteristics are described in Section 2. Section 3 describes the empirical study. Finally, research results and concluding remarks are given in section 4.

Table 2
Sn63Pb37 compared with lead-free SAC alloy candidate.

Properties	Leaded (Sn63Pb37)	Lead-free (Sn96.5/Ag3.0/Cu0.5)	Unit
Solder paste properties			
Melting point	183	217	°C
Surface tension	420	450 to 500	mN/M
Tensile strength	41	35	mPa
Shearing strength	27	30	mPa
Hardness	13	15	Hv
Density	8.5	7.4	g/cm^3
Shelf life (In refrigeration)	>12	12	Month
Shrinkage effects	Low	High	–
Cosmetics	Shiny	Dull	–
Relative cost	1×	3×	–
Self-centering during reflow	Good	Fair	–
Important reflow soldering criteria			
Reflow process window	67–77	48–53	°C
Minimum preheat Temp.	100	150	°C
Maximum preheat Temp.	150	200	°C
Reflow lower Temp. limit	200	235 °C	°C
Reflow upper Temp. limit	235	245 to 260	°C
Reflow peak Temp.	205–215	235–245	°C

2. Literature review

2.1. Taguchi method

The Taguchi method is widely utilized to determine factor level combination and to evaluate possible factor interactions thereby ensuring the appropriate design of a product or process [37]. This methodology allows process practitioners to initiate experiments with many factors varying on a few levels instead of necessitating full factorial experiments [42]. The orthogonal array (OA) and signal-to-noise (S/N) ratios are the main instruments for economically conducting and analyzing an experiment. The OA is a fractional factorial matrix where the process factors are arranged into columns and the factor level combinations are designed by rows to be used for the experimental runs. The S/N ratio is used to evaluate deviation from the target of a response and process varia-

tion [36] with a higher S/N ratio indicating a more robust process. However, the Taguchi method emphasizes single response optimization. In practice, an engineer's subjective judgment is required to optimize a process with multiple quality characteristics using a weighting approach. It is troublesome and unreliable for engineers to decide on a definite weight for each response.

Taguchi defined three attributes of quality characteristics to transform responses into S/N ratios [37,2], including: (1) the smaller-the-better (STB); (2) the larger-the-better (LTB); and (3) the nominal-the-better (NTB). The attributes LTB and NTB adopted in this study are formulated as shown in Eqs. (1) and (2) to obtain the respective S/N ratios.

$$\mathrm{S/N_{STB}} = -10\log_{10}\left(\frac{\sum_{i=1}^{n} y_i^2}{n}\right) \tag{1}$$

$$\mathrm{S/N_{NTB}}(\eta) = 10\log_{10}\left(\frac{\mu^2}{\sigma^2}\right)$$
$$\text{where}\mu = \frac{y_1 + y_2 + y_3 + \cdots + y_n}{n} \tag{2}$$
$$\sigma^2 = \frac{\sum_{i=1}^{n} (y_i - \bar{y})^2}{n-1}$$

2.2. Fuzzy logic system

The fuzzy set theory introduced by [56] was designed to manipulate the imprecise and vague information proceeding from the human decision-making process by using the degree of membership [24]. This method can be used to quantitatively tackle decisions stipulating uncertain parameters [23]. For example, a fuzzy set A in X corresponds to a type of membership function $\mu_A(x)$ which indicates the grade of membership of x in A within the interval [0,1]. A is defined as $\{(x, \mu_A(x)) \mid x \in X\}$ on a universe of discourse X [24]. The fuzzy logic system is inspired by fuzzy set theory and enables the modeling of the human reasoning process. This is a universal approximator for the implementing of nonlinear mapping between input vectors into scalar outputs in terms of firing fuzzy rules to some degree [27]. The fuzzy logic system and fuzzy reasoning have been successfully adopted in many complex industrial applications [12,52,48].

Fuzzy logic systems have frequently been utilized for process simulation or control. The systems can be constructed either based on expert knowledge or from data based on a set of "If-Then" rules [27]. A typical fuzzy logic system has four ingredients, including the fuzzifier, fuzzy rule base, inference engine, and defuzzifier. First, in the fuzzification process, the crisp inputs are fuzzified into linguistic variables using membership functions. In the fuzzy inference process, the fuzzy implications are implemented by the composition of fuzzy relations, such as max-min and max-product compositions. The max-min composition provides superior leverage and is compromised of fuzzy rules that yield a more reasonable reasoning result [21], and is used in this study.

In the simple two two-input and one-output fuzzy rules are considered:

R_1: IF x_1 is A_1 and x_2 is B_1 THEN y is C_1;

R_2: IF x_1 is A_2 and x_2 is B_2 THEN y is C_2.

To combine these two rules to infer C, the max-min composition is utilized and illustrated as in Eq. (3).

$$\mu_c(y) = [\mu_{A_1}(x_1) \wedge \mu_{B_1}(x_2) \wedge \mu_{C_1}(y)] \vee [\mu_{A_2}(x_1) \wedge \mu_{B_2}(x_2) \wedge \mu_{C_2}(y)], \tag{3}$$

where μ_A, μ_B, and μ_C represent the membership functions of A_1, B_1, and C_1, respectively. The symbol "$\wedge$" is the minimum aggregation, and "$\vee$" is the maximum aggregation.

In defuzzification the fuzzy output is converted into a crisp value. The center of area (CoA) is a widely-used defuzzification method which calculates the area under the scaled membership functions corresponding to the limit of the output variable and generates a crisp value [41], defined as Eq. (4) below:

$$CoA = \frac{\sum_{j=1}^{n} \mu_A(z_j) z_j}{\sum_{j=1}^{n} \mu_A(z_j)}, \tag{4}$$

where $\mu_A(z)$ is the output membership function.

2.3. Genetic algorithm

Genetic algorithm (GA) was invented to mimic the process of a natural evolution system to parallelly and globally resolve optimization problems using the mechanism of natural selections [16], which empowers its capability of resolving both constrained and unconstrained optimization problems. Comparing with conventional searching techniques, GA can simultaneously and quickly assess many points and simulate the survival of the fittest among individuals across the solution space, therefore is more likely to obtain the global solution.

Initially, GA starts with a set of candidates called a population, and followed by repeat modifications for a population of individual solutions through "evolves" for achieving the optimal solutions. The evolving process involves include selection, crossover, and mutation operators. The selection mechanism randomly selects the individuals and survival of the fittest. The crossover operator represents mating between individuals. The mutation introduces random modifications. Interested readers are referred to Coley [11] to obtain a more detailed discussion of the GA and its applications. The GA pseudo codes are listed as below.

Randomly choose initial population
Evaluate each fitness of individual
Do loop
Select the fittest individuals to reproduce
Mate pairs randomly
Apply crossover operator (P_c)
Apply mutation operator (P_m)
Evaluate each fitness of individual
Until terminating condition is met

2.4. Artificial neural network

Artificial neural network (ANN) is a commonly used artificial intelligence tool that mimics the decision-making process of a biological neural system. ANN is a powerful modeling tool to map the nonlinear relationship between multiple inputs and multiple outputs through data learning [9]. The back-propagation network (BPN) is a popular supervised data-leaning algorithm that adjusts randomized weights using the steepest gradient descent method along the error surface during the data learning process [38]. Some of the user-defined parameters used to design a BPN model include: (1) the number of input, hidden, and output layers; and the number of processing nodes for each layer; (2) the learning rate; and (3) the momentum. Readers are referred to Lippmann [25] for the general design rules for modeling a BPN.

In the last two decades, ANN has been utilized to solve prediction [19], functional approximation [3], and process control and optimization problems [35,8,28]. Due to the nonlinear nature and complexity of the fine-pitch micro-BGA stencil printing process, the BPN algorithm is suitable to establish the nonlinear relationship

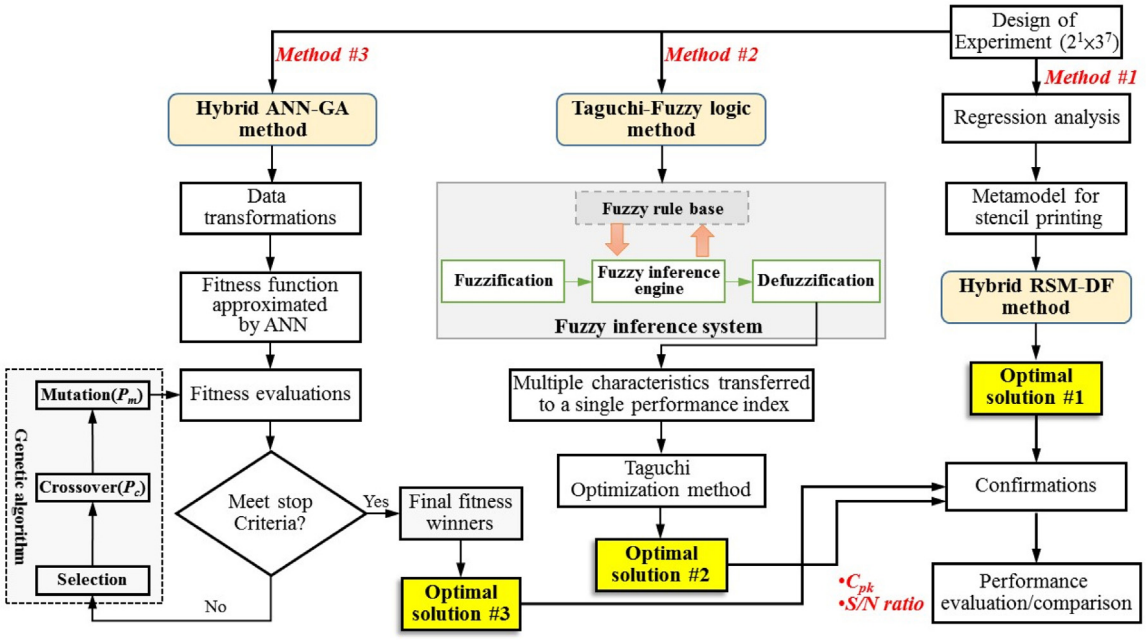

Fig. 2. Flow diagram of optimization of the stencil printing process.

between process inputs and outputs. The hybrid method combines ANN and GA can be an alternate to resolve the given optimization problem in this study, that is, the trained BPN patterns acts as the fitness function for the genetic algorithm to optimally search the micro-BGA stencil printing parameter sets.

2.5. Response surface methodology

Response surface methodology (RSM) is a series of mathematical and statistical techniques used for system modeling and analysis [32]. By a design of experiment (DOE), the objective is to optimize responses which are influenced by several input variables using a two or three-dimension hyper surface. Generally, the second-order (or *quadratic*) model is given by Eq. (5), which is one of the frequently-used models for optimizing the given problem presented in this study.

$$Y = \beta_0 + \sum_{i=1}^{n} \beta_i x_i + \sum_{i=1}^{n} \sum_{j=1}^{n} \beta_{ij} x_i x_j + \varepsilon \tag{5}$$

where $(x_1, x_2, \cdots, x_n)$ represent the input parameters, $(\beta_1, \beta_2, \cdots, \beta_n)$ are the estimated coefficients, β_0 denotes the mean of all responses, and ε is a random error component.

Previous applications of the Taguchi method mostly considered a single quality characteristic for stencil printing process, so a simultaneous optimization solution on multiple performance characteristics is deficient. Additionally, many researchers have attempted to solve the problem of ensuring stencil printing quality using statistical analysis [34,33,5], artificial intelligence [26,46] and mathematical modeling [50,53]. Although some improvements

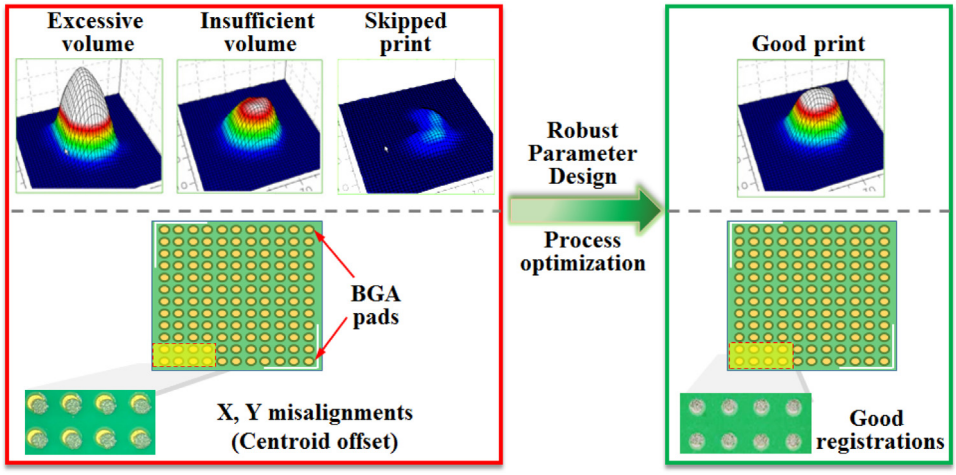

Fig. 3. SPI images for a BGA package.

Table 3
Stencil printing factors.

Printing factors	Descriptions
Separation speed	The speed setting for separating PCB and stencil after a printing cycle.
Wiping frequency	The frequency of stencil cleaning using a wiper after a specified number of PCBs have been printed.
Squeegee pressure	Pressure applied on the squeegee to control the printed pattern and solder paste volume.
Squeegee speed	Speed the squeegee moves across the stencil surface to transfer solder paste onto solder pads.
Snap-off height	Distance between the stencil and PCB for controlling the amount of solder paste deposited.
Stencil aperture ratio	Ratio of the aperture area to the area of the pad.
Stencil thickness	Thickness of a stencil used to control solder paste volume.
Paste viscosity	Changes in viscosity during printing, which controls printing pattern.

Table 4
Factor levels of stencil printing parameters.

Abbreviations;	Factors	Level I	Level II	Level III
A (Sep_speed)	Separation speed (mm/sec)	1.0	3.0	–
B (Wipe_F)	Stencil wiping frequency (cycles/times)	1	3	5
C (S_ press)	Squeegee pressure (kg)	5	7	9
D (S_speed)	Squeegee speed (mm/sec)	20	40	60
E (Snap_off)	Snap-off height (mm)	0	0.5	1.0
F (R_ratio)	Stencil aperture ratio (%)	90%	100%	110%
G (S_thick)	Stencil thickness (mm)	0.08	0.10	0.12
H (Viscosity)	Solder paste viscosity (kcps)	900	1100	1300

have been made in certain aspects, emphasis should still be placed others:

(1) There are contradictions that need to be clarified with conflicting conclusions reached, especially for determining which influential factors are significant to the stencil printing process [26,34,51].
(2) Most previous investigations focused on a few stencil printing factors so may not provide practical solutions for manufacturers.
(3) Investigating only one response makes it difficult to obtain robust process parameters. It may be impractical to evaluate the overall relationships between the factors that influence the stencil printing process and multiple characteristic quality empirically.
(4) The Taguchi method has frequently been applied to optimize the stencil printing parameters. However, there is some degree of uncertainty related to the STB, LTB, and NTB attributes involving "more or less" judgments using the Taguchi method [55].

The micro-BGA stencil printing process has multiple quality characteristics. We therefore propose three hybrid optimization methods to resolve the multi-response optimization problem for the fine-pitch micro-BGA stencil printing due to a synergistic alliance of dichotomous methods could yield optimization strategies inheriting the advantages and problem-solving capabilities of the diverse parent methods [30,31,47]. Finally, the optimization performance of these three methods were compared through conformation experiments.

3. Empirical illustrations

This work uses as a case study an anonymous electronic manufacturing service (EMS) provider in southern Taiwan, referred to here as company O. The subject company fabricates many types of data servers, wireless products (e.g., routers and Bluetooth modules), and computer accessories. According to quality reports, engineers have long been plagued by process variability and soldering defects in the micro-BGA packages, including solder voids, solder shorts, and head-in-pillow defects. The quality and reliability of the electronic products are dependent upon reliable solder joints and are closely related to the stencil printing results.

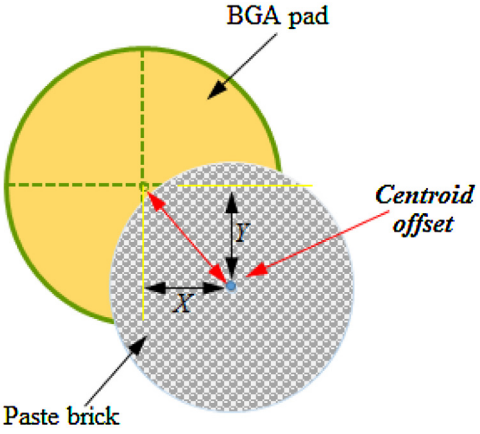

Fig. 4. Measuring the centroid offset of a solder paste brick for BGA.

To comprehensively resolve the stencil printing process optimization problem for micro-BGA packages, the three optimization methods are proposed and compared, as shown in Fig. 2. Considering the economic issue, a structured data set was collected from a fractional factorial experimental design containing eight factors and two responses. In the first method, the experimental data were meta-modelled through multiple regression analysis to derive two equations for the responses. The optimal parameter combinations were then derived using the integration of RSM and DF. Method #2 combines the multiple quality characteristics into a single performance index using a fuzzy logic system after which the Taguchi method is used to acquire the optimal parameter settings. Method #3 establishes an ANN model that formulates the nonlinear relationships of the stencil printing by training the experimental data followed by the application of the GA to search for the optimal parameter sets. The steps in the optimization process are described in detail below.

Table 5
L18 Orthogonal array and the responses.

Exp. run	Control factors								Responses		Responses-S/N ratios (db)	
	A	B	C	D	E	F	G	H	Volume (y_1)	Centroid offset (y_2)	Volume (η_1)	Centroid offset (η_2)
#1	1	1	1	1	1	1	1	1	487	5.99	29.2	−15.9
#2	1	1	2	2	2	2	2	2	617	6.77	30.5	−16.6
#3	1	1	3	3	3	3	3	3	917	23.43	29.0	−27.5
#4	1	2	1	1	2	2	3	3	755	5.16	26.7	−14.7
#5	1	2	2	2	3	3	1	1	602	15.68	25.2	−24.1
#6	1	2	3	3	1	1	2	2	499	19.35	30.4	−25.9
#7	1	3	1	2	1	3	2	3	713	6.15	25.8	−16.5
#8	1	3	2	3	2	1	3	1	707	18.55	31.0	−25.5
#9	1	3	3	1	3	2	1	2	433	17.49	23.6	−25.0
#10	2	1	1	3	2	2	2	1	706	14.27	30.0	−23.4
#11	2	1	2	1	1	3	3	2	881	6.33	26.9	−16.5
#12	2	1	3	2	2	1	1	3	487	18.17	23.7	−25.5
#13	2	2	1	2	3	1	3	2	812	11.31	30.6	−21.4
#14	2	2	2	3	1	2	1	3	521	14.48	25.1	−23.4
#15	2	2	3	1	2	3	2	1	641	13.55	23.8	−22.8
#16	2	3	1	3	2	3	1	2	692	14.52	25.0	−23.3
#17	2	3	2	1	3	1	2	3	614	15.51	28.5	−21.4
#18	2	3	3	2	1	2	3	1	705	17.08	26.8	−24.8
Mean									654.9	13.5	27.3	−21.9

Table 6
Fuzzy rules for MCPI.

		Solder paste volume				
		Very_low	Low	Medium	High	Very_high
Centroid offset	Very_low	Tiny	Very_small	Small	S_Medium	Medium
	Low	Very_small	Small	S_Medium	Medium	M_Large
	Medium	Small	S_Medium	Medium	M_Large	Large
	High	S_Medium	Medium	M_Large	Large	Very_Large
	Very_high	Medium	M_Large	Large	Very_Large	Huge

3.1. Experimental design

The quality improvement team utilized a fishbone diagram to identify important factors and investigate the cause-and-effect of stencil printing for the micro-BGA package based on the categories of man, machine, materials, methods, measurement, and work environment (5M1E). The eight factors were selected based on the literature review and expert knowledge, and supplemental off-line experiments to achieve reliable solder paste bricks for the micro-BGA packages. These factors are summarized and briefly explained in Table 3. The factor level for each parameter is set and illustrated in Table 4. The underlined values are the initial factor levels set for mass production.

The desired amount of solder paste volume and centroid offset are the two most significant characteristics to ensuring the print quality for micro-BGA packages in the stencil printing process [40]. To assess the performance of the stencil printing process, an automated 3D solder paste inspection (SPI) machine is usually installed to precisely monitor and measure solder paste volume and paste-to-pad alignments. The multiple quality characteristics of a BGA package stencil printing process including solder paste volume and centroid offset are measured and depicted in Fig. 3.

The specifications of the two responses (i.e., solder paste volume and centroid offset rate) were defined in conformity with expert knowledge and the industry standards [17], listed as follows:

Solder paste volume for a micro-BGA package (16×16, 0.5-mm lead pitch): The specification is 600 mil^3 with a tolerance +/−100 mil^3. It has the attribute of NTB.

Centroid offset: The centroid offset is calculated by measuring the distance between the center of the solder paste print and its associated BGA pad using Eq. (6) as shown in Fig. 4. The offset has the attribute of LTB.

$$Centroidoffset = \sqrt{X^2 + Y^2} \tag{6}$$

The OA used in the experiment is illustrated on the left part of Table 5. Each experimental run was randomly conducted with five replications. The MPM UP 3000 stencil printer and laser-cut stainless stencils were utilized in the experiment. The paste deposit volume was measured using an automated 3D SPI machine. The volume and centroid offset of the micro-BGA package was measured by averaging 5 bricks deposited at the four corners and the center of the pads. The S/N ratios of these two responses are summarized on the right part of Table 5. The main effects of the S/N ratios for the responses are shown in Fig. 5, which are used in the Taguchi method to determine the optimal parameter settings individually.

The optimal factor level for solder paste volume is set to be $A_1B_1C_1D_3E_3F_1G_3H_2$, whereas the optimal setting for centroid offset is $A_1B_1C_1D_1E_1F_2G_2H_2$. Apparently, incompatibility exists between the two factor level combinations. That is, the Taguchi method cannot synchronously optimize the stencil printing process with multiple quality characteristics without determining the weights of responses based on the judgment of experts.

3.2. Process parameter optimization using RSM and desirability function

The quadratic regression models for paste volume and centroid offset are constructed and illustrated in Eqs. (7) and (8), respectively. The ANOVA results show the p-values for volume and offset centroid are 0.043 and 0.0028, respectively. The two p-values are less than 0.05 implying both the two models are significant [29]. Additionally, the R-squared and adjusted R-squared values for these

Response table for solder paste volume

	A	B	C	D	E	F	G	H
Level 1	27.95	28.22	27.88	26.45	27.37	28.91	25.28	27.69
Level 2	26.70	26.96	27.86	27.10	26.79	27.10	28.18	27.82
Level 3		26.79	26.23	28.42	27.81	25.96	28.50	26.46
Effect	1.24	1.43	1.65	1.97	1.02	2.95	3.22	1.36
Rank	7	5	4	3	8	2	1	6

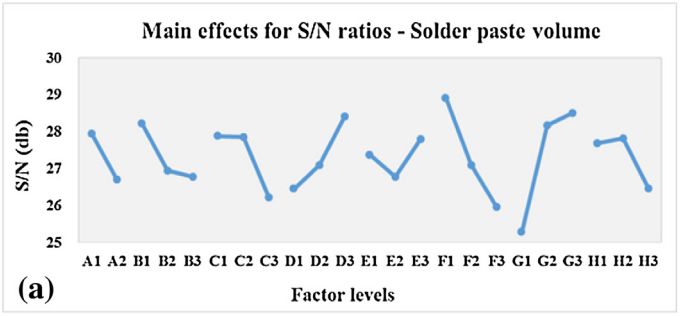

Response table for solder paste centroid offset

	A	B	C	D	E	F	G	H
Level 1	-21.3	-20.9	-19.2	-19.4	-20.5	-22.6	-22.8	-22.7
Level 2	-22.5	-22.0	-21.2	-21.5	-21.4	-21.3	-21.1	-21.4
Level 3		-22.7	-25.2	-24.8	-23.8	-21.8	-21.7	-21.5
Effect	1.21	1.86	6.07	5.44	3.31	1.30	1.74	1.29
Rank	8	4	1	2	3	6	5	7

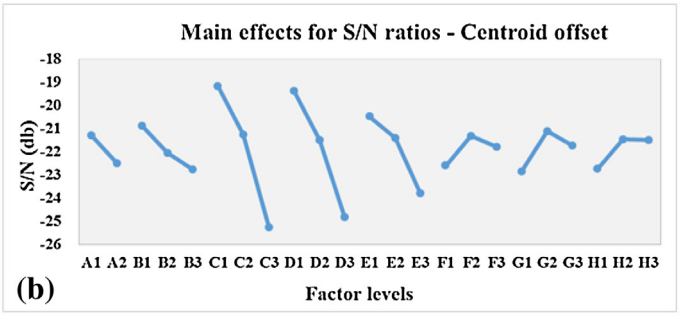

Fig. 5. Response tables and plots of main effects for (a) solder paste volume and (b) centroid offset.

two models are larger than 0.90 indicating they demonstrate good interpolation capability in the process modeling.

$$Volume = 618.7685 + 23.1667 \times A + 10.4722 \times B + 1.2515 \times C - 0.7353 \times D + 2.7940 \times E + 60.6119 \times F + 111.0139 \times G - 6.4498 \times H - 20.7160 \times AC - 7.4460 \times AF - 13.1667 \times FH - 15.8194 \times C^2 \quad (7)$$

Table 7
Summary of the MCPIs for each experiment run.

Exp. run	S/N- Volume	S/N- Offset	MCPI-1 MBF: Triangular	MCPI-2 MBF: Trapezoidal	MCPI-3 MBF: Gaussian	Rank
#1	29.25	−15.86	0.8572	0.8611	0.8638	2
#2	30.52	−16.63	0.9001	0.9025	0.9001	1
#3	29.05	−27.48	0.4410	0.4302	0.4325	10
#4	26.68	−14.68	0.6507	0.6517	0.6512	5
#5	25.18	−24.07	0.1744	0.1729	0.1462	16
#6	30.42	−25.90	0.5000	0.5007	0.5001	8
#7	25.81	−16.49	0.5807	0.5846	0.5947	6
#8	31.03	−25.48	0.5000	0.5007	0.5001	8
#9	23.56	−24.98	0.0999	0.0796	0.1001	17
#10	29.98	−23.36	0.5650	0.5749	0.5774	7
#11	26.86	−16.45	0.6651	0.6721	0.6777	3
#12	23.66	−25.50	0.0999	0.0796	0.1001	17
#13	30.57	−21.39	0.6637	0.6663	0.6755	4
#14	25.05	−23.37	0.1886	0.1846	0.1841	14
#15	23.84	−22.84	0.1910	0.1851	0.1991	13
#16	24.99	−23.31	0.1864	0.1821	0.1849	15
#17	26.66	−21.44	0.4114	0.5675	0.5712	11
#18	26.83	−24.78	0.2627	0.2610	0.2738	12

Table 8
ANOVA results for the MCPI.

Source	Sum of Squares	*df*	Mean Square	*F*-value	*p*-value	Contributions (%)
Model	0.931531	8	0.116441	6.3292549	0.006078	–
A	0.120083	1	0.120083	6.5271769	0.030948	12.89%
B	0.184314	1	0.184314	10.0184967	0.011454	19.79%
C	0.303754	1	0.303754	16.5107445	0.002828	32.61%
D	0.020361	1	0.020361	1.10673852	0.320217	2.19%
E	0.040705	1	0.040705	2.21255404	0.171065	4.37%
F	0.052483	1	0.052483	2.8527724	0.125483	5.63%
G	0.207192	1	0.207192	11.262039	0.008444	22.24%
H	0.00264	1	0.00264	0.14351715	0.713592	0.28%
Residual	0.165576	9	0.018397			
Total	1.097107	17				

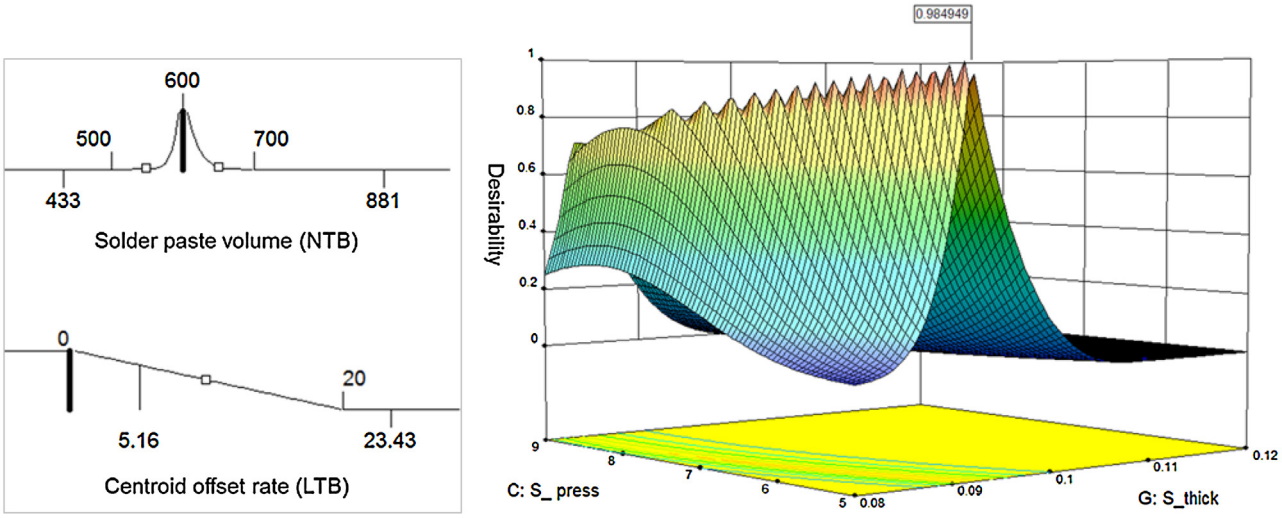

Fig. 6. Optimization criteria and contour plot for desirability (Squeegee pressure vs. stencil thickness).

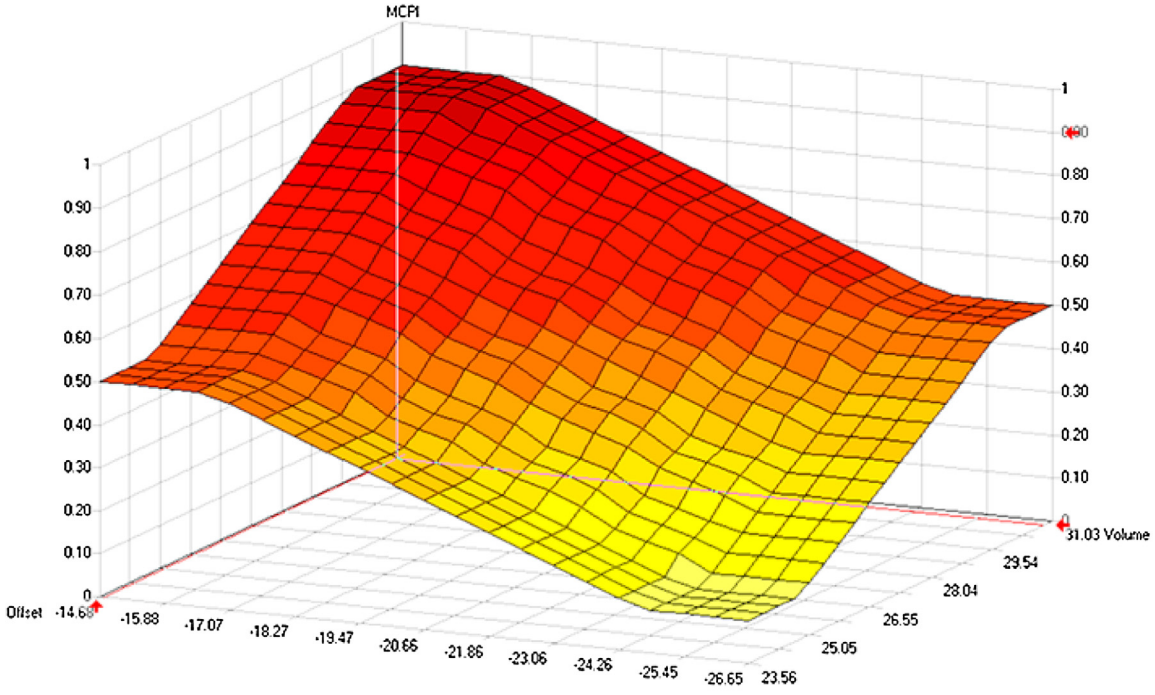

Fig. 7. Surface contour for the proposed fuzzy logic system.

$$Offset = 12.6283 + 2.605 \times B + 4.3058 \times C + 2.7658 \times D + 1.6542 \times E - 0.185 \times H + 2.82 \times CH + 1.3733 \times H^2 \quad (8)$$

To resolve the multi-response problem, a numerical model can be used to find optimal points through maximizing the DF [32]. The DF ranges from 0 to 1 at the goal. All the importance weights of the goals can be adjusted and combined into one overall desirability function $D(X)$ [13], as in Eq. (9) below

$$D = (d_1 \times d_2 \times \cdots \times d_n)^{\frac{1}{n}} = \left(\prod_{i=1}^{n} d_i\right)^{\frac{1}{n}}, \quad (9)$$

where n stands for is the number of responses in the measure.

For targeting the goal, the desirability is defined as follows:

$$d_i = \begin{cases} d_i = 0, y_i \le Low_i \\ d_i = \left[\dfrac{y_i - Low_i}{High_i - Low_i}\right]^{wt_i}, Low_i < y_i < T_i \\ d_i = 1, y_i = T_i \\ d_i = \left[\dfrac{High_i - y_i}{High_i - T_i}\right]^{wt_i}, T_i < y_i < High_i \\ d_i = 0, y_i \ge High \end{cases}, \quad (10)$$

where wt denotes the importance weight of a goal.

For the goal of minimum, the desirability is defined as follows:

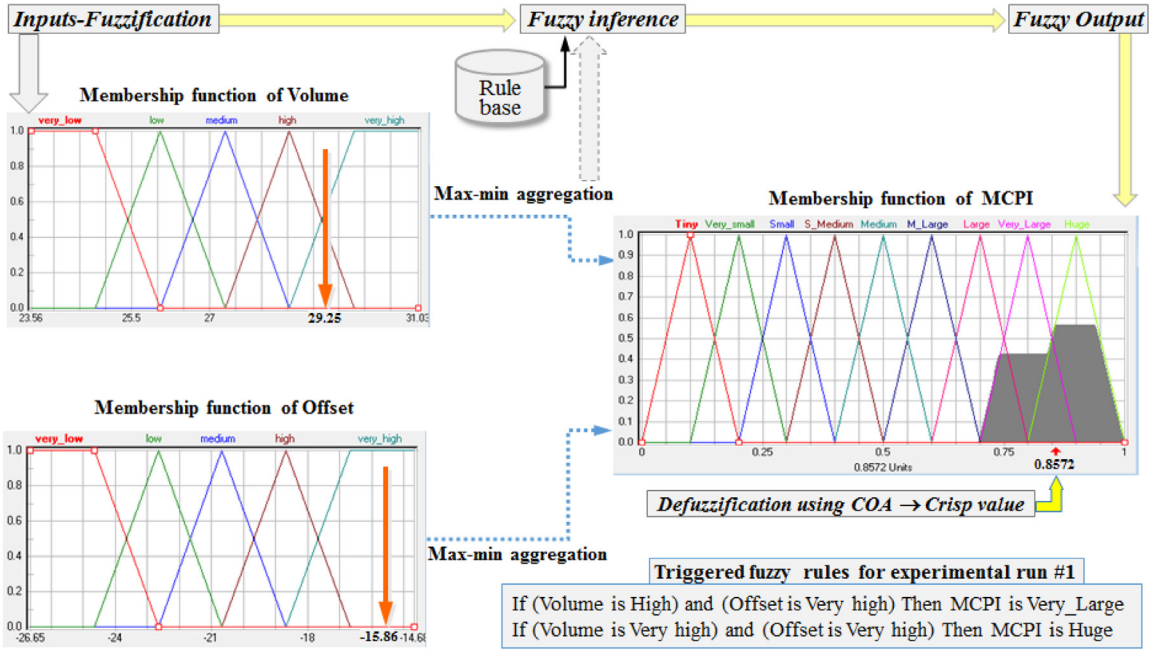

Fig. 8. Fuzzy logic system.

$$(11) d_i = \begin{cases} d_i = 1, y_i \le Low_i \\ \left[\dfrac{High_i - y_i}{High_i - Low_i}\right]^i, Low_i < y_i < High_i \\ d_i = 0, y_i \ge High \end{cases}.$$

One can change the shape of the desirability of each goal by adjusting its weight to emphasize the upper bounds, the lower bounds, or the target. In this study, the DFs of the solder paste volume and the centroid offset rate are defined by Eqs. (12) and (13), respectively. The weight for the lower bound of the solder paste volume is more important than that of the upper bound since a lower amount of solder paste volume can result in voids or incomplete solder joints leading to a more expensive quality recovery cost.

$$d_{\text{volume}} = \begin{cases} 0, y_{\text{volume}} < 500 \\ \left(\dfrac{y_{volume} - 500}{200}\right)^{10}, 500 \le y_{\text{volume}} \le 600 \\ \left(\dfrac{700 - y_{volume}}{100}\right)^{5}, 600 < y_{\text{volume}} \le 700 \\ 0, y_{\text{volume}} > 700 \end{cases} \quad (12)$$

$$d_{\text{offset}} = \begin{cases} 1, y_{\text{offset}} = 0 \\ \left(\dfrac{20\% - y_i}{20\%}\right), 0 < \hat{Y}_{\text{offset}} \le 20\% \\ 0, y_{\text{offset}} > 20\% \end{cases} \quad (13)$$

Design-Expert® (V9.0) [14] is used to optimize the multi-response optimization problem. The input factors are set in the ranges of the factor levels, while targeting the solder paste volume (600 mil^3) and minimizing the centroid offset rate. The optimization criteria for the two responses are graphically depicted in the left part of Fig. 6. The surface contour is demonstrated in the right part of Fig. 6. The highest desirability achieved is 0.985. Therefore, the optimum parameter combination is: A (stencil separation speed: 2.3 mm/s), B (wiping frequency: 1 time/cycle), C (squeegee pressure: 5 kg), D (squeegee speed: 21 mm/s), E (snap-off distance: 0 mm), F (stencil are ratio: 105%), G (stencil thickness: 0.09 mm), and H (paste viscosity: 1170 kcps). The optimal parameter settings are summarized in the second column of Table 9.

	A	B	C	D	E	F	G	H
Level 1	0.523	0.588	0.584	0.479	0.509	0.505	0.268	0.425
Level 2	0.359	0.395	0.473	0.447	0.421	0.445	0.525	0.503
Level 3		0.340	0.266	0.397	0.393	0.373	0.531	0.395
Effect	0.163	0.248	0.318	0.082	0.116	0.132	0.263	0.107
Rank	4	3	1	8	6	5	2	7

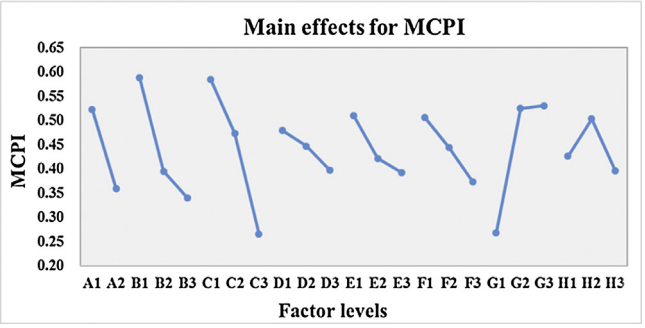

Fig. 9. Response table and main effects for the MCPI.

3.3. Process parameter optimization using Fuzzy logic and the Taguchi method

The S/N ratios for the volume and centroid offset are transferred into a multiple characteristics performance index (MCPI) using the proposed fuzzy logic system, followed by using Taguchi method to derive the optimal parameter combination. The Mamdani-type fuzzy logic system is employed to deal with real-valued inputs and outputs of the stencil printing process. The triangular, trapezoidal, and Gaussian types of membership functions (MBFs) were evaluated in this study. The MBFs of the two inputs are defined by five terms, whereas the MCPI is set to ten terms to obtain a more precise result. A number of fuzzy rules ($5 \times 5 = 25$) are generated and

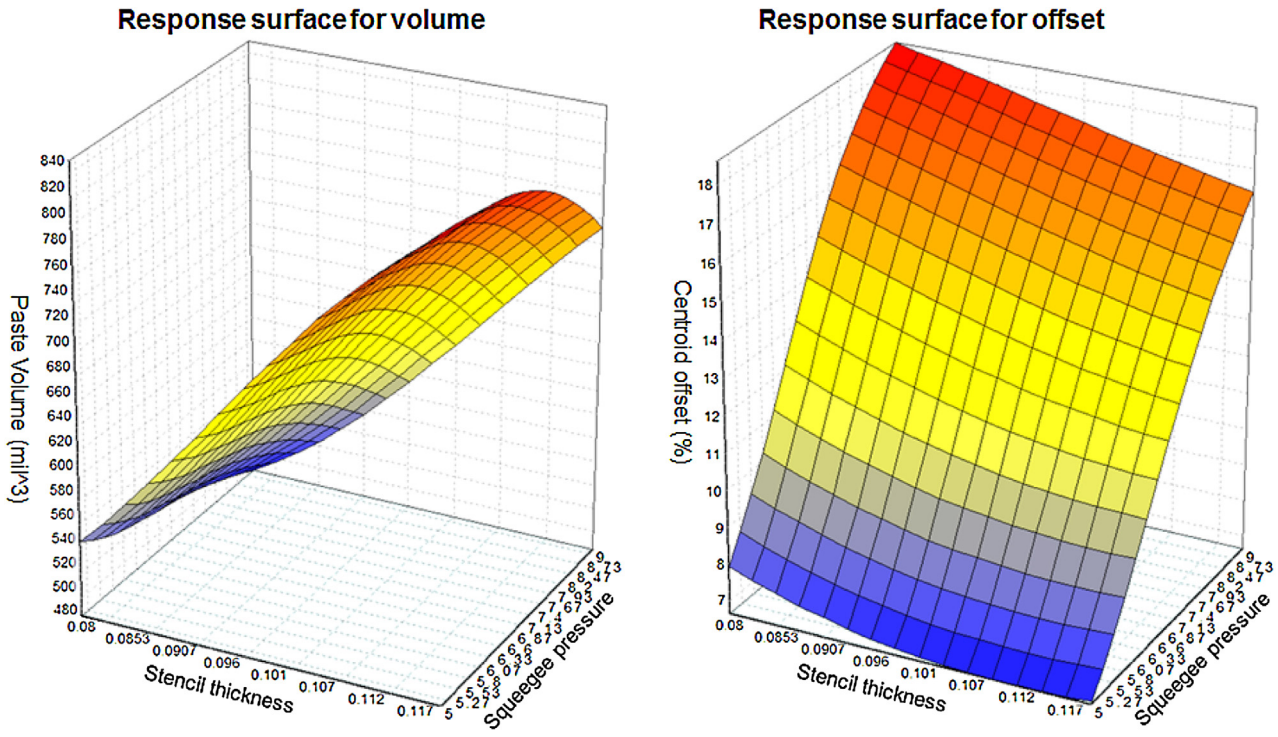

Fig. 10. Response surface plots for volume and offset (squeegee pressure vs. stencil thickness).

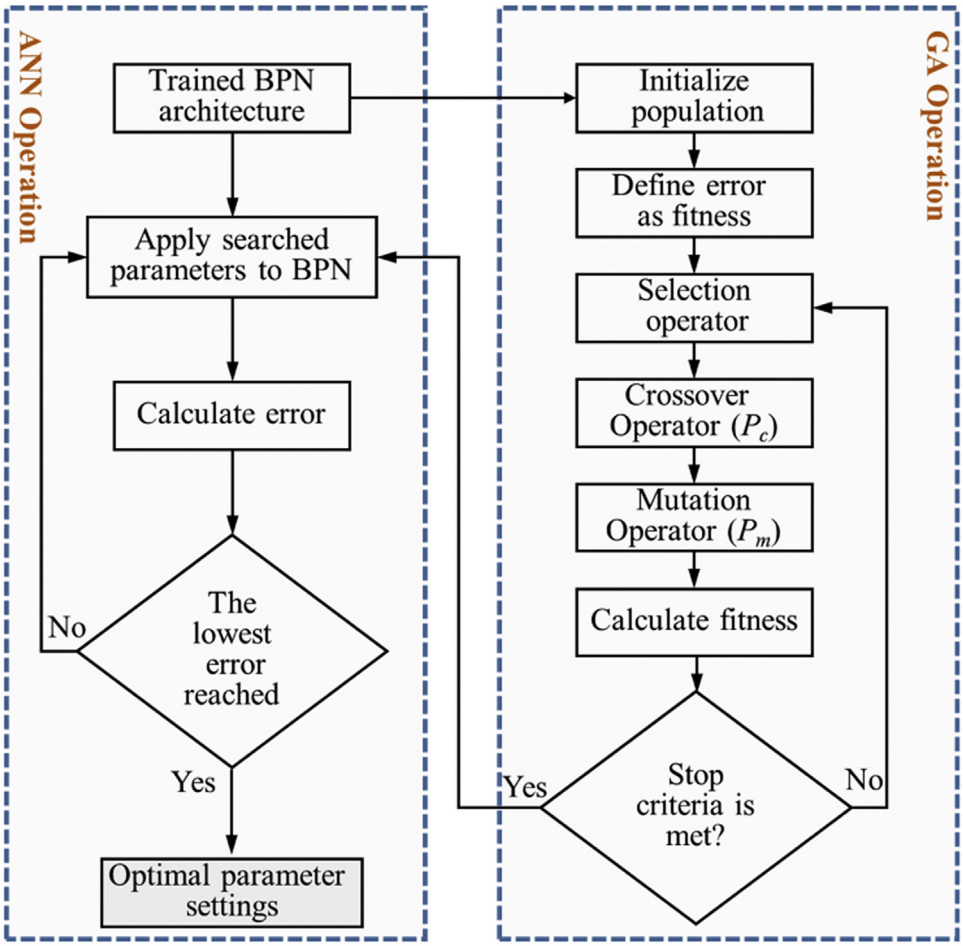

Fig. 11. ANN-GA operation chart.

Table 9
Optimal parameter settings derived from the three methods.

Methods Parameters	RSM-DF (solution #1)	Taguchi-Fuzzy logic (solution #2)	ANN-GA (solution #3)
Separation speed	2.30	1.00	1.00
Wiping frequency	1.00	1.00	2.00
Squeegee pressure	5.00	5.00	5.40
Squeegee speed	21.00	20.00	20.00
Snap-off height	0.00	0.00	0.00
Aperture ratio	105.00	90.00	90.00
Stencil thickness	0.09	0.12	0.10
Solder paste viscosity	1170	1100	1260

Table 10
Results of confirmation experiments.

Methods KPI	Initial condition (mass production)	Optimum parameter settings					
		RSM-DF		Fuzzy-Taguchi		ANN-GA	
		Confirmation	Improvement PIR (%)	Confirmation	Improvement PIR (%)	Confirmation	Improvement PIR (%)
Volume	27.16 dB	30.62 dB	12.74%	33.48 dB	**23.27%**	31.58 dB	16.27%
Centroid	−23.37 dB	−19.36 dB	17.15%	−16.95 dB	**27.47%**	−19.74 dB	15.53%
Volume-*Cpk*	0.78	1.15	–	**1.57**	–	1.30	–
Centroid-*Cpk*	1.09	1.60	–	**2.38**	–	1.21	–

summarized in Table 6 [49], which are used to transform multiple quality characteristics into a performance index (i.e., the MCPI). The COA defuzzification method (illustrated in Eq. (4)) is used to derive a crisp value for each experimental run. The contour and the mechanisms of the fuzzy logics system using the triangular MBFs are depicted in Fig. 7 and Fig. 8. Taking experimental run #1 as an example, the S/N input for volume is 29.25 and centroid offset is −15.86; the crisp MCPI 0.8572 is acquired after COA defuzzification.

The resulting MCPIs for all the experimental runs are summarized in Table 7. The ranks of MCPIs transformed by the three fuzzy logic systems using different fuzzy MBFs are identical. Experimental run #2 has the highest MCPI value and perceivably is the best factor level combination. The response table and main effects of the MCPIs are shown in Fig. 9. The optimum parameter setting $A_1B_1C_1D_1E_1F_1G_3H_2$ is achieved by: A (stencil separation speed: 1.0 mm/sec), B (wiping frequency: 1 time/cycle), C (squeegee pressure: 5 kg), D (squeegee speed: 20 mm/sec), E (snap-off distance: 0 mm), F (stencil ratio: 90%), G (stencil thickness: 0.12 mm), and H (paste viscosity: 1100 kcps). The optimal parameter settings are summarized in the second column of Table 7. The response table and main effects of the MCPIs are shown in Fig. 9. The ANOVA for the MCPI is illustrated in Table 8.

The model is significant with a *p*-value is less than 0.05. Additionally, an adjusted *R*-squared value of 84.91 implying the model can reliably be used to interpolate [29]. The model is significant with A (separation speed), B (wiping frequency), C (squeegee pressure), and G (stencil thickness) are the significant model terms. The contribution of each factor is indicated in the last column of Table 8: the squeegee pressure (32.61%) is considered the most significant contributor, followed by stencil thickness (22.24%), wiping frequency (19.79%), and separation speed (12.89%).

3.4. Process parameter optimization using ANN and GA methods

In this hybrid optimization method, the BPN is utilized to nonlinearly formulate the relationship between process inputs and outputs, while the trained BPN model acts as the fitness function which is evaluated by a GA searching process to derive the optimal parameter settings using the NeuralPower® (2003) software package. Firstly, the experimental data are normalized into a range from 0 to 1 prior to development of the BPN model. There are no universally accepted rules of thumb to design a BPN topology which depends on the tradeoff between mapping accuracy and computational complexity. The design of the BPN model is two-fold. First, the default BPN modeling parameters of NeuralPower® (the learning rate is 0.8 and momentum is 0.8) are used, and 1 hidden layer and 1 output layer with the *Sigmoid* transfer function were designated to train the experimental data with a limit of 10,000 iterations. The 18 sets of experimental data are randomly assigned into a training data set (80%, 14 sets) and a testing group (20%, 4 sets). The modeling errors are measured using the root-mean-square-error (RMSE). An ANN topology "8-11-2" with the lowest RMSE is derived through trial-and-error examinations. The resulting ANN topology with 8 input neurons, 11 neurons for the hidden layer, and 2 neurons for the output layer is achieved with the lowest RMSE (0.0023) after the pilot runs.

In the second phase, the learning rate and momentum are evaluated and optimized based on the predetermined "8-11-2" network topology. The resulting parameters are the learning rate (set at 0.3) and momentum (set at 0.5) from which the lowest RMSE (0.0009) and a shorter elapsed time in convergence are gained. Again, the model is verified using a non-repeating 20% of the test samples for 5 runs. The mapping accuracy is evaluated through the average RMSE and the correlation coefficient (*R*) as defined in Eq. (14). The closer the correlation coefficient approaches to 1, the higher the correlation between process inputs and responses. The verification results exhibit an average *R* that is close to 1 and an average RMSE that is close to 0 for both responses (i.e., volume and centroid offset) indicating the achievement of high modeling accuracy. The response surface plots for both responses are depicted in Fig. 10.

$$R = \frac{\sum_{i=1}^{n}(Q_i - \bar{Q})(q_i - \bar{q})}{\sqrt{\sum_{i=1}^{n}(Q_i - \bar{Q})^2 (q_i - \bar{q})^2}}, \tag{14}$$

where $\bar{Q} = \frac{1}{n}\sum_{i=1}^{n} Q_i$, $\bar{q} = \frac{1}{n}\sum_{i=1}^{n} q_i$; Q_i is the *i*th training sample data; and q_i denotes the predictions.

The established BPN model then acts as the objective function in the GA search process for finding the optimum parameter sets, as illustrated in Fig. 11. The desired volume is set at 600 mil^3 and minimizing the centroid offset rate is expected. A vector of floating

numbers with the lower and upper bounds of the inputs is represented by a chromosome. The tournament selection strategy is utilized to search for the best fitness of crossover operation based on preliminary tests and the uniform crossover with the real-value coding are used. The initial population size is set to be 80 to ensure the efficiency of the searching process and prevent premature convergence. Each chromosome is evaluated by the fitness function using the trained BPN model. The results are evaluated for the entire population and to obtain the ranked fitness values.

According to the pseudo codes listed in section 2, the GA parameters (the crossover rate (P_c) and the mutation rate (P_m)) are tuned using a preliminary 2^3 experiment design with three replications. Each GA parameter is set at three levels. The level settings of crossover probability are 0.3, 0.5, and 0.7, whereas the three levels of mutation probability are 0, 0.2, and 0.4. As a result, the optimal GA parameter setting ($P_c = 0.5$, $P_m = 0.4$) is acquired based on the least sum of absolute error. Therefore, P_c is set to 0.5, P_m is set to 0.4 and the tournament selection strategy is utilized in the GA evolutionary process. Finally, the optimum stencil printing parameter settings for the BGA packages are obtained as illustrated in the last column of Table 9.

3.5. Confirmation experiments and the comparison of optimization performance

Confirmation experiments were conducted to verify the degree of improvement for the micro-BGA stencil printing quality and offer empirical assurance of the optimization performance of the three methods. The optimal parameter settings derived by the three methods are summarized in Table 9 with each optimal parameter set replicated six times in the experiments. The S/N ratios and *Cpk* are the indicators used to evaluate the optimization performance. A performance improvement rate (*PIR*) is defined in Eq. (15) for comparison with the initial condition of mass production. The results of performance comparison are summarized in Table 10. Obviously, the proposed Taguchi-fuzzy logic method outperforms the other two methods, in terms of both the S/N ratios and *Cpk*.

$$PIR(\%) = \frac{[\text{ConfirmedS/Nratio} - \text{InitialconditionS/Nratio}]}{\text{IntitalconditionS/Nratio}} \times 100 \quad (15)$$

The results of the confirmation experiments demonstrate that: (1) the merger of the Taguchi method and fuzzy logic system improves the S/N ratios for deposited volume and centroid offset by 23.27% and 27.47%, respectively, compared to the initial settings used in mass production; (2) the fuzzy logic-based Taguchi method is better than the other two methods for resolving the multi-response problem; and (3) all three methods provide satisfactory optimization performance compared to the initial conditions for mass production.

4. Results and concluding remarks

Stencil printing is the most important process in SMA but exhibits complex behaviors which can increase soldering defects which can lead to significant loss of quality and production time. In particular, soldering defects have become more prevalent and are difficult to detect for BGA packages in the process of lead-free assembly and can require costly quality recovery efforts. One approach to increasing first pass yield and reducing manufacturing costs is to optimize the process of solder paste printing and its multiple quality characteristics before the failures are detected in the downstream manufacturing steps.

To solve the parameter optimization problem for the fine-pitch micro-BGA stencil printing with multiple quality characteristics, a fuzzy logic-based Taguchi method is proposed. The method is used to derive robust parameter settings which are then compared with those obtained with two other hybrid methods. The evaluation results show the fuzzy logic-based Taguchi methodology can practically optimize the process. With the proposed fuzzy logic-based Taguchi method: (1) minimal experimental data can be applied to formulate the nonlinear relationships of process inputs and outputs without considering the overfitting problem; (2) the proposed method is capable of synthesizing the multi-objectives into a single performance index for solving a multi-response optimization problem simultaneously; (3) the proposed method relieves the difficulties of determining the importance weight of each response and the uncertainty involved in the decision-making process; and (4) the proposed systematic analysis tools are easily implemented in related mixture optimization problems. To further advance the optimization performance, different optimization methods (e.g., Monte Carlo simulation, ant colony optimization, and nonlinear mathematical programming) can be applied in future.

Acknowledgements

The authors would like to thank the subject company for providing related support and the Ministry of Science and Technology in Taiwan for supporting this research under Contract No. MOST 103-2410-H-366-003-MY2.

References

[1] A. Al-Refaie, Optimizing SMT performance using comparisons of efficiency between different systems technique in DEA, IEEE Trans. Electron. Packag. Manuf. 32 (4) (2009) 256–264.
[2] C. Ahilan, S. Kumanan, N. Sivakumaran, J.E.R. Dhas, Modeling and prediction of machining quality in CNC turning process using intelligent hybrid decision making tools, Appl. Soft Comput. 13 (3) (2013) 1543–1551.
[3] O. Arndt, T. Barth, B. Freisleben, M. Grauer, Approximating a finite element model by neural prediction for facility optimization in groundwater engineering, Eur. J. Oper. Res. 166 (2005) 769–781.
[5] L.G. Barajas, M.B. Egerstedt, E.W. Kamen, A. Goldstein, Stencil printing process modeling and control using statistical neural networks, IEEE Trans. Electron. Packag. Manuf. 30 (1) (2008) 9–18.
[6] L. Bruno, T. Johnson, Solder paste printing: quality assurance methodology, SMT Mag. 30 (5) (2015) 28–46.
[7] D. Bušek, K. Dušek, D. Růžička, M. Plaček, P. Mach, J. Urbánek, J. Starý, Flux effect on void quantity and size in soldered joints, Microelectron. Reliab. 60 (5) (2016) 135–140.
[8] S. Chanda, S. Gupta, D.K. Pratihar, A combined neural network and genetic algorithm based approach for optimally designed femoral implant having improved primary stability, Appl. Soft Comput. 38 (1) (2016) 296–307.
[9] R.P. Cherian, L.N. Smith, P.S. Midha, A neural network approach for selection of power metallurgy materials and process parameters, Artif. Intell. Eng. 14 (2000) 29–44.
[10] W.E. Coleman, Critical parameters for stencil performance, SMT Mag. 22 (2) (2008) 27–29.
[11] D.A. Coley, An Introduction to Genetic Algorithms for Scientists and Engineers, World Scientific, Singapore, 1999.
[12] O. Cordon, A historical review of evolutionary learning methods for Mamdani-type fuzzy rule-based systems: designing interpretable genetic fuzzy systems, Int. J. Approx. Reason. 52 (2011) 894–913.
[13] G. Derringer, Suichd, Simultaneous optimization of several response variable variables, J. Qual. Technol. 12 (1980) 214–219.
[14] Design-Expert Software Version 9.0 User's Guide 2015.
[15] Fleck, P. Chouta, A new dimension in stencil print optimization, J. SMT 16 (2003) 24–33.
[16] E.D. Goldberg, Genetic Algorithms in Search, Optimization and Machine Learning, Addison-Wesley, Reading, MA, 1989.
[17] IPC-A-610 rev. D-Acceptability of Electronic Assemblies. 2004 November.
[18] JEDEC/Electronic Industries Alliance, Inc, Moisture/Reflow Sensitivity Classification for Non-Hermetic Solid State Surface Mount Devices, March 2008.
[19] S. Kanmani, V.R. Uthariaraj, V. Sankaranarayanan, P. Thambidurai, Object-oriented software fault prediction using neural networks, Inf. Softw. Technol. 49 (2007) 483–492.
[20] Z. Khan, Ball Grid Array Soldering, Assembly Magazine, 2008 http://www.assemblymag.com/articles/85323-ball-grid-array-soldering.
[21] B.Y. Lee, Y.S. Tarng, Surface roughness inspection by computer vision in turning operations, Int. J. Mach. Tools Manuf. 41 (2001) 1251–1263.
[22] L.M. Lee, A.A. Mohamad. Interfacial reaction of Sn–Ag–Cu lead-free solder alloy on Cu: a review Adv. Mater. Sci. Eng. 2013; 2013, 11 http://dx.doi.org/10.1155/2013/123697 Article ID 123697.

[23] T.F. Liang, H.W. Cheng, P.Y. Chen, K.H. Shen, Application of fuzzy sets to aggregate production planning with multiproducts and multitime periods, IEEE Trans. Fuzzy Syst. 19 (3) (2011) 465–477.
[24] C.-T. Lin, C.S.G. Lee, Neural Fuzzy Systems: A Neuro-fuzzy Synergism to Intelligent Systems, Prentice Hall, NJ, 1996.
[25] R.P. Lippmann, An introduction to computing with neural nets, IEEE Acoust. Speech Signal Process. Mag. 4 (1987) 4–22.
[26] A. Lofti, M. Howarth, Industrial application of fuzzy systems: adaptive fuzzy control of solder paste stencil printing, Inf. Sci. 107 (1998) 273–285.
[27] M. Luo, K. Zhang, Robustness of full implication algorithms based on interval-valued fuzzy inference, Int. J. Approx. Reason. 62 (2015) 61–72.
[28] A. Mariajayaprakash, T. Senthilvelan, R. Gnanadass, Optimization of process parameters through fuzzy logic and genetic algorithm—a case study in a process industry, Appl. Soft Comput. 30 (5) (2015) 94–103.
[29] S. McKillup, Probability Helps You Make a Decision About Your Results, Statistics Explained: An Introductory Guide for Life Scientists, 1st ed., Cambridge University Press, Cambridge, United Kingdom, 2006, pp. 44–56.
[30] Z. Michalewicz, M. Schmidt, M. Michalewicz, C. Chiriac, Adaptive Business Intelligence, Springer, Berlin Heidelberg, 2006.
[31] M.S.S. Mir, J. Rezaeian, A robust hybrid approach based on particle swarm optimization and genetic algorithm to minimize the total machine load on unrelated parallel machines, Appl. Soft Comput. 41 (4) (2016) 488–504.
[32] R.H. Myers, D.C. Montgomery, C.M. Anderson-cook, Response Surface Methodology—Process and Product Optimization Using Designed Experiments, John Wiley & Sons, Hoboken, NJ, 2009.
[33] E.S. Pan, Y. Jin, Z. Mei, Y. Wang, A two-stage optimization method for the stencil printing process based on neural network and response surface method, Adv. Mater. Res. 156–157 (2010) 10–17.
[34] J. Pan, G.L. Tonkay, R.H. Storer, R.M. Sallade, R.J. Leandri, Critical variables of solder paste stencil printing for micro-BGA and fine-pitch QFP, IEEE Trans. Electron. Packag. Manuf. 27 (2004) 125–132.
[35] M. Pacella, O. Semeraro, Using recurrent neural networks to detect changes in autocorrelated process for quality monitoring, Comput. Ind. Eng. 52 (2007) 502–520.
[36] M.S. Phadke, Quality Engineering Using Robust Design, AT&T Bell Labs, 1989.
[37] P.J. Ross, Taguchi Techniques for Quality Engineering, McGraw-Hill, NY, 1996.
[38] D.E. Rumelhart, G.E. Hinton, R.J. Williams, Learning internal representations by error propagation, in: Parallel Distribution Processing: Explorations in Microstructure of Cognition, MIT press, Cambridge, MA, 1986.
[39] K. Seelig, Head-in-Pillow BGA Defects, AIM, Solder, Montreal Canada, 2008 http://www.aimsolder.com/sites/default/files/head-in-pillow_bga_defects.pdf.
[40] C. Shea, A new SPI tool for defect prevention Printed Circuit Design & Fab Circuits Assembly. 32 (1) 2015, 26–39.
[41] S. Shaw, Fuzzy Control of Industrial Systems: Theory and Applications, Springer Science, NY, 1998.
[42] T.V. Sibalija, V.D. Majstorovic, Z.D. Miljkovic, An intelligent approach to robust multiresponse process design, Int. J. Prod. Res. 49 (17) (2011) 5079–5097.
[43] Smith, Advances in fine-pitch printing process technology, Circuits Assembly (2014) 30–36.
[44] W. Stęplewski, G. Kozioł, J. Borecki, Influence of stencil design and parameters of printing process on lead-free paste transfer efficiency, in: XXXII International Conference of IMAPS – CPMT IEEE, Poland, 21–24 September, Pułtusk, 2008.
[45] T.-N. Tsai, Modeling and optimization of stencil printing operations: a comparison study, Comput. Ind. Eng. 54 (3) (2008) 374–389.
[46] T.-N. Tsai, Improving the fine-pitch stencil printing capability using the Taguchi method and Taguchi fuzzy-based model, Rob. Comput. Integr. Manuf. 27 (4) (2011) 808–817.
[47] T.-N. Tsai, A hybrid intelligent approach for optimizing the fine-pitch copper wire bonding process with multiple quality characteristics in IC assembly, J. Intell. Manuf. 25 (1) (2014) 177–192.
[48] J.-H. Yeh, T.-N. Tsai, Optimizing the fine-pitch copper wire bonding process with multiple quality characteristics using a grey-fuzzy Taguchi method, Microelectron. Reliab. 54 (1) (2014) 294–303.
[49] Y.-F. Tzeng, F.C. Chen, Multi-objective optimization of high-speed electrical discharge machining process using a Taguchi fuzzy-based approach, Mater. Des. 28 (2007) 1159–1168.
[50] G.S. White, C.J.W. Breward, P.D. Howell, R.J.S. Young, A model for the screen-printing of Newtonian fluids, J. Eng. Math. 54 (1) (2006) 49–70.
[51] M. Whitmore, C. Mackay, A. Hobby, Plastic stencils for bottom-side chip attach, Electron. Packag. Prod. 37 (13) (1997) 68–72.
[52] B.K. Wong, V.S. Lai, A survey of the application of fuzzy set theory in production and operations management: 1998–2009, Int. J. Prod. Econ. 129 (2011) 157–168.
[53] T. Wright, Mathematical modeling of solder paste stenciling for process control, Circuits Assembly 18 (2) (2007) 75–80.
[54] T. Yamamoto, K.-I. Tsubone, Assembly technology using lead-free solder, Fujitsu Sci. Techn. J. 43 (1) (2007) 50–58.
[55] Y.-S. Yang, W. Huang, A grey-fuzzy Taguchi approach for optimizing multi-objective properties of zirconium-containing diamond-like carbon coatings, Expert Syst. Appl. 39 (2012) 743–750.
[56] L.A. Zaheh, Fuzzy sets, Inf. Control 8 (1965) 338–353.